Laser and Particle Beams (2006), *24*, 395–401. Printed in the USA.

DOI: 10.1017/S0263034606060551

An inductive scheme of power conditioning at mega-Ampere currents

A.S. CHUVATIN,[1] V.A. KOKSHENEV,[2] L.E. ARANCHUK,[1] D. HUET,[3]
N.E. KURMAEV,[2] AND F.I. FURSOV[2]

[1]Laboratoire de Physique et Technologie des Plasmas, Ecole Polytechnique, Palaiseau, France
[2]High Current Electronics Institute, Tomsk, Russia
[3]Centre d'Etudes de Gramat, Gramat, France

(RECEIVED 2 January 2006; ACCEPTED 27 March 2006)

Abstract

This work describes an inductive energy storage scheme intended for power multiplication at mega-Ampere currents. The key power multiplication element of the scheme is an opening switch generating the voltage of inductive origin. The switch represents an additional volume with magnetically accelerated solid-state or plasma conductor between the generator and the load. Motion of the conductor increases the inductance of the volume. A sufficiently fast increase of this inductance at the end of magnetic energy storage time ensures power multiplication. A critical requirement for the accelerated conductor is the possibility of temporal profiling of the inductance increase. A proof-of-principle experiment at GIT12 shows that such profiling is possible. We suggest a simple analysis of the scheme efficiency and illustrate this analysis for a multi-mega-Ampere class generator. The scheme is alternative to existing inductive energy storage technologies for pulsed-power conditioning at high currents.

Keywords: Inductive energy storage schemes; Pulse power

1. INTRODUCTION

Mega-Ampere currents with the rise-time substantially less than one microsecond would allow the next generation of plasma radiation sources to appear (Davis *et al*., 1996; Matzen, 1997). Compression of fast plasma liners envisaged for this goal would contribute to radiation production, high energy density physics, and inertial confinement fusion research. A possible way to reach these high currents consists in using the inductive energy storage principle (IES). This principle implies that a low-impedance fast capacitor bank produces a microsecond-duration current I_0 in a storage inductance. Further operation of a power multiplication element converts a part of the stored magnetic energy into electric energy. A high voltage U_z is thus generated across the load and ensures the load current rise-time to be smaller than that of the generator.

However, the problem of such a power multiplication element for mega-Ampere IES generators is far from being solved. Several technologies were already studies for the mentioned fast energy conversion, such as magnetic flux compressors (Megagauss, 1990), plasma flow switches (Turchi *et al*., 1987), exploding foils or wires, or plasma opening switches (IEEETPS, 1987). In particular, the last two schemes use interesting properties of materials or plasmas to interrupt abruptly high currents at the end of the time necessary for magnetic energy storage. Despite these fuses, or opening switches do allow current pulse sharpening, their maximum impedance (of dissipative origin) scales to decrease with increasing maximum storage current, I_0 (Chuvatin *et al*., 1997). This results in limited voltage generated by the fuse, while the voltage at a pulse power load with constant impedance scales as $U_z \propto I_0$.

In contrast with the resistive switches, it was suggested to use the voltage of inductive, rather than dissipative origin both at high-impedance (Rudakov, 1999), and low-impedance (Chuvatin, 1999; Chuvatin *et al*., 2002) pulse power generators. In this paper, we discuss a particular configuration, where staged acceleration could allow both successful magnetic energy storage at low initial impedance and rapid transfer of this energy into an inductive load when the impedance increases.

Address correspondence and reprint requests to: Alexandre Chuvatin, Laboratoire de Physique et Technologie des Plasmas, Ecole Polytechnique, 91128 Palaiseau, France. E-mail: chuvatin@lptp.polytechnique.fr and chuvatin@yahoo.com

2. INDUCTIVE SWITCHING SCHEME

Consider configuration shown in Figure 1 for cylindrical geometry. Two inductances, L_z of the load and L_0 of the additional volume are connected electrically in parallel through the convolute 3. Both inductances are powered by a low-impedance microsecond capacitor bank 1 (C, L_g). The connector 5 is open during the capacitor discharge. The current through the conductor 4 with the initial mass M reaches its maximum value I_0. The conductor is accelerated axially by the $j \times B$ force up to high velocity. This results in variation of the associated conductor inductance L_p from its initial value L_0. When the conductor reaches the end of the axial acceleration region and goes beyond, the mass of the conductor starts to expand to the large vacuum cavity 6. This may results in interruption of electrical contact of this mass with the electrodes. Or, a small current-carrying portion of the conductor mass m is formed, and it is further magnetically accelerated toward the axis. In both cases, inductive voltage $I_0 \times dL_p/dt$ is generated across the load 2. At this moment, the closing switch 5 connects the load to the rest of the circuit and the magnetic energy is transferred into the inductance L_z.

One should address two important issues here. First, the electrode geometry in Figure 1 is chosen to provide $L_p \ll L_g$ and $dL_p/dt \ll (L_g/C)^{1/2}$ at the axial stage of the conductor motion. This must ensure efficient current transfer from a low-impedance generator to the conductor volume. Second, consider the motion of possible residual conductor mass m. The impedance dL_p/dt associated with radial acceleration of this small mass is higher than that appearing during the axial acceleration of the whole mass M. In contrast with the other type of fuses or opening switches mentioned above, the impedance dL_p/dt arising during radial acceleration may be proportional to the maximum current I_0 or, at least, remains constant. This scaling is typical for radially imploded fast z-pinches (Matzen, 1997 and the references therein) and suggests potential applicability of the scheme at mega-Ampere currents.

The staged axial-to-radial acceleration is typical for plasma flow switch geometries (Turchi *et al.*, 1987). In the plasma flow switch, however, a part of the conductor mass is supposed to bring the current to the load. The configuration of Figure 1 suggests a different scenario: the moving conductor operates as an opening switch in parallel to the load and does not penetrate into the load region.

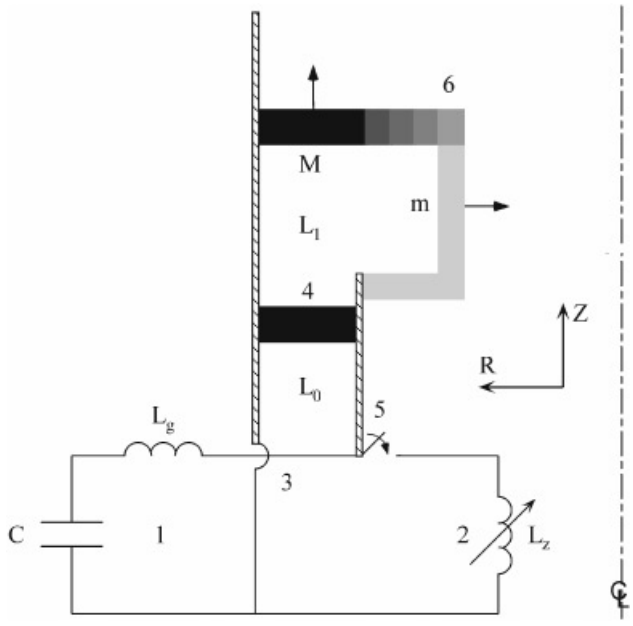

Fig. 1. Inductive switch arrangement in the considered electrical circuit. 1—capacitor bank, 2—inductive load, 3—convolute, 4—initial position of a conductor, 5—closing switch, 6—conductor expanding into vacuum, its inductance L_p changes from L_0 to L_1. M—the main conductor mass, m—possible residual conducting mass.

3. EXPERIMENT ON STAGED ACCELERATION

Therefore, a critical assumption for efficient operation of the scheme of Figure 1 is that the electrode geometry provides $L_p \approx L_0 \ll L_g$ during the magnetic energy storage time (typically of the order of 1 μs for modern low-impedance capacitor banks) and that the conductor inductance subsequently increases to the value $L_1 \gg L_0$. Also, an inductive voltage must be generated by the accelerating and expanding conductor in order to allow power multiplication and further current transfer to a load if the latter is connected.

Validation of these criteria for the geometry of Figure 1 was performed on GIT12 generator (Kovalchuk *et al.*, 1997) at the current level of 2–3 MA. The terminal part of GIT12 was modified as shown in Figure 2. Moderate level of the available generator current and hence limited maximum mass of the conductor 4 in Figure 1 did not allow usage of azimuthally homogeneous shells. The conductor in Figure 2 is organized by 12 tungsten 11 μ-diameter wires tighten horizontally at the initial position 4 between the cathode, $R_c = 10$ cm, and the anode, $R_a = 13$ cm. The acceleration distance between the wires and the exit to the large volume 6 is 4 cm.

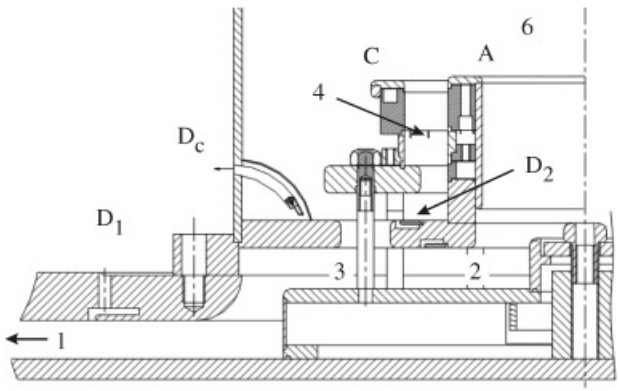

Fig. 2. Experimental arrangement on GIT12. C—cathode, A—anode, D_1, D_c, D_2—dI/dt probes for measurements of the currents I_1, I_c, and I_2, respectively. Other notations are the same as in Figure 1.

https://doi.org/10.1017/S0263034606060551 Published online by Cambridge University Press

The GIT12 generator *1* is equivalent to a capacitor, C = 14.4 μF, an active resistance of 0.04 Ohm and a storage inductance (up to the D_1 probe position), L_g = 89 nH. Geometrical inductance between D_1 and the convolute 3 is L_v = 11.3 nH. Corresponding value for the part between the convolute and the initial wire position 4 is L_0 = 7.8 nH. The voltage U_s is measured at the bottom of a 424 nH mechanical support (not shown in Fig. 2) and then inductively corrected. Therefore, the voltage values corresponding to the convolute, U_c, and to the initial wire position, U_p, as well as the varying wire array inductance during the shot, L_p, can be evaluated as follows:

$$U_c = U_s - L_v \times D_1, \quad U_p = U_c - L_0 \times D_2,$$

$$L_p(t) = \int U_p\, dt/I_2. \tag{1}$$

Figure 3 shows experimental result on the temporal profiling of the inductance L_p. The convolute current I_c becomes negative indicating intense (> 1 MA) current losses, presumably under the form of electron beams provoked by the plasma radiation. The convolute current is measured as the average of three D_c probe signals and it is sensitive to the vacuum current. The convolute leakages effectively act as a vacuum diode load in parallel to the inductive part and they lead to the I_2 current drop.

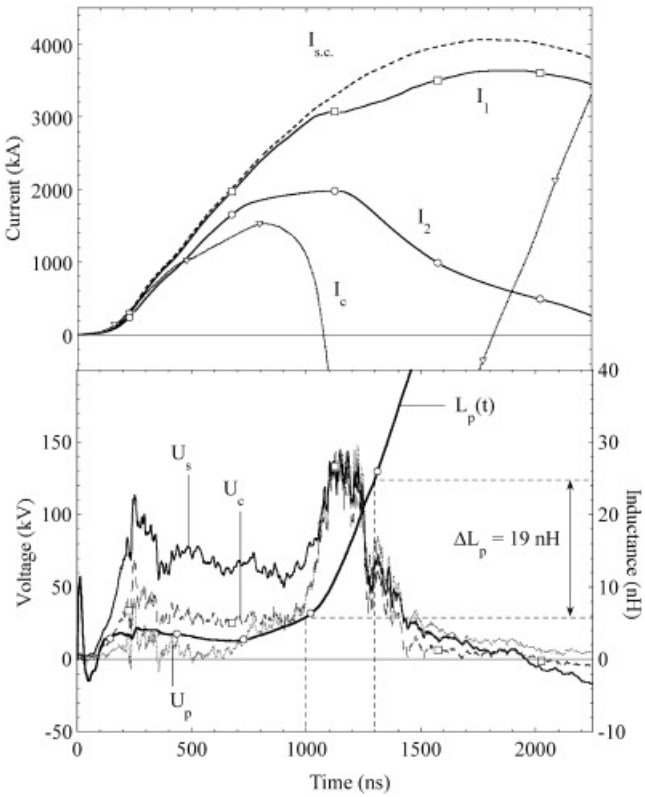

Fig. 3. Measured currents upstream, I_1, and downstream, I_2, of the convolute in a wire array shot. I_c—convolute current. Measured, U_s and inductively corrected, U_c and U_p, voltages in the same shot, as well as the inductance evaluated from experimental results with the help of Eq. (1). $I_{s.c.}$—current of all the probes in a calibration shot with a short circuit at the position 4 in Figure 2.

The results of Figure 2 confirm that the chosen geometry of electrodes allows maintaining low values of $L_p \approx L_0$ during the microsecond magnetic energy storage time. Later in time, a voltage pulse is generated having amplitude at the convolute of ~130 kV. The conductor inductance, evaluated by Eq. (1), increases by approximately 20 nH during 300 ns, and reaches the value of ~25 nH. Therefore, the chosen geometry of electrodes allows efficient coupling with a low-impedance capacitor bank and further generation of the voltage of inductive origin.

An undesirable but predictable effect in the described setup is that the conductor mass is limited by the limited number of wires. The inter-wire distance appears to be almost twice larger than the anode-cathode gap. This may not allow formation of a compact conducting shell and can lead to relatively slow plasma precursor formation (Lebedev *et al*., 1997; Aleksandrov *et al*., 2003, 2004; Sinars *et al*., 2004) instead of acceleration of the whole mass. However, apparently successful $L_p(t)$ staging in Figure 3 and appearance of the voltage multiplication in the experiment suggest that the scheme is further improvable. Usage of very high number of wires (Mazarakis *et al*., 2004) or of thin foils (Nash *et al*., 2004) at higher energies may allow either keeping the conductor thickness close to the initial thickness of a solid-state foil (as in the explosively driven magnetic flux compression experiments, Megagauss, 1990), or reaching theoretical limit for a plasma shell thickness, $\Delta z \sim \delta_{sk}$, where δ_{sk} is the magnetic field skin-depth (Rudakov *et al*., 2003). Higher shell compactness would provide higher dL_p/dt values to be reachable.

4. IDEAL SCHEME EFFICIENCY

Let us perform a simple analysis on the scheme shown in Figure 1. As shown the experiment, motion of the conductor 4 in Figures 1 and 2 can be presented by variable inductance $L_p(t)$ changing from its initial value L_0 to the final value L_1. This inductance is almost constant at the inductive storage stage. This allows the energy stored in the capacitor C to be converted into magnetic energy in the inductance $L_g + L_0$. Full energy conversion occurs at the time moment equal to the quarter-period τ of the capacitor discharge in LC circuit:

$$\tau = \pi\sqrt{(L_g + L_0)C}/2. \tag{2}$$

Consider further rapid change of the inductance L_p and simultaneous connection of the load 2 in Figure 2. For the sake of simplicity, we consider an inductive load with constant inductance L_z = const. The load is connected at the moment when the inductance L_p starts to rise. Neglecting the energy dissipation, the magnetic flux in the circuit at this moment is further conserved, and it is equal to the magnetic

https://doi.org/10.1017/S0263034606060551 Published online by Cambridge University Press

flux at the moment when $L_p = L_1$ and when the load current is equal to I_z. This provides us with the following current transfer coefficient:

$$k \equiv \frac{I_z}{I_0} = \frac{L_1 - L_0}{L_1 + L_2 + \dfrac{L_1 L_z}{L_g}}. \quad (3)$$

Here I_0 is the generator current at $L_p = L_0$, I_z is the load current at $L_p = L_1$. The energy efficiency coefficient is therefore defined as

$$\eta \equiv \frac{E_z}{E_0} = \frac{L_z}{L_g + L_0} k^2. \quad (4)$$

Here E_0 is the initial stored energy and E_z is the magnetic energy in the load inductance. For $L_z = L_g$, $L_0 \to 0$ and $L_1 \to \infty$ we have $\eta = 0.25$ (25 % efficiency) and $k = 0.5$ (half of the stored current is transferred into the load).

The further logic is the following. The circuit parameters defining feasibility of a pulse power system using the configuration of Figure 1 are L_1 (defining the efficiency of inductive switching), the capacitor bank erecting voltage V, and the duration of the inductive storage phase τ, Eq. (2). To optimize the system, let us consider the function $\eta(L_g)$. Its maximum occurs at

$$L_g^{opt} = \frac{4L_0}{\sqrt{1 + 8(L_0/L_z + L_z/L_1)} - 1}. \quad (5)$$

The other important characteristic is the $V\tau$ product, which should be preferably minimized (smaller charging voltages reduce the risk of electric breakdowns and smaller generator current rise-times result in smaller subsequent load current rise-times):

$$V\tau = \frac{\pi}{2} I_0 (L_g + L_0). \quad (6)$$

Therefore, for a fixed load inductance and for fixed inductive switch inductances L_0 and L_1, Eqs. (5) and (6) define the maximum energy transfer efficiency $\eta(L_g^{opt})$ and the parameter $V\tau$.

5. EXAMPLE OF A MEGA-AMPERE GENERATOR

Consider parameters of a pulse power system with inductive load. For example, one could estimate $L_z = 5$–7 nH as the mean load inductance of a fast z-pinch (Davis *et al.*, 1996; Matzen, 1997). Figure 4 shows calculated values of $\eta(L_g^{opt})$ and $V\tau(L_g^{opt})$ for the load with $L_z = 7$ nH, $I_z = 60$ MA and for different values of $\Delta L = L_2 - L_1$.

One can see that the increase of L_0 considerably decreases the maximum efficiency η and increases $V\tau$. For example, the value $L_0 = 4$ nH (corresponds to the inductance of electrical connections with the initial conductor position 4 in Fig. 1) yields to $\eta > 10\%$ for $\Delta L > 30$ nH. From the results of Figure 4 and for the case of $L_1 = 40$ nH, one could derive generator characteristics shown in Table 1.

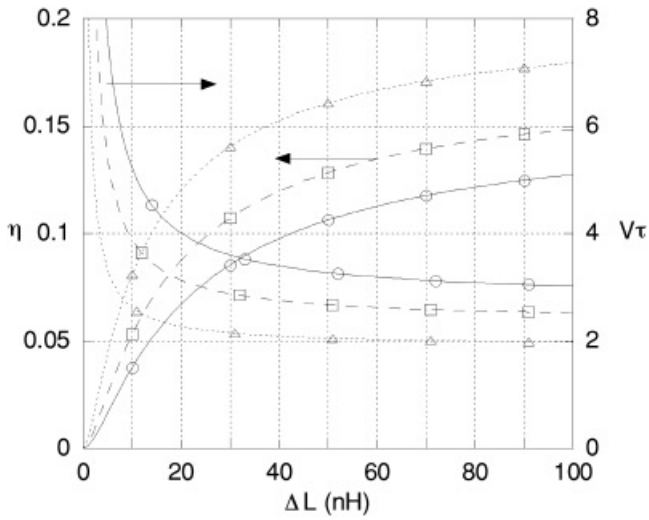

Fig. 4. Efficiency η and the parameter $V\tau$ (in MV × μs) for $L_0 = 2$ nH (triangles), $L_0 = 4$ nH (squares) and $L_0 = 6$ nH (circles). The load inductance is $L_z = 7$ nH.

For a microsecond capacitor bank discharge, the primary generator voltage can be maintained at the level of 2–3 MV, i.e., at the values acceptable for existing technologies of microsecond capacitor banks.

The scheme of Figure 1 allows parallel connection of inductive volumes as schematically shown in Figure 5. This relaxes the requirement on the output voltage of the primary generator. For example, at unchanged performance of the scheme (i.e., same I_z, τ, L_0, and L_1), each capacitor bank is characterized by the parameters shown in Table 2.

6. ELECTRICAL CIRCUIT MODEL

Modeling of the electrical circuit of Figure 1 was performed for a z-pinch-type load. Equivalent circuit corresponding to the scheme of Figure 1 can be represented by the following set of equations:

Table 1. *Generator parameters calculated from Figure 4 for the scheme shown in Figure 1*

Primary store	Inductive switch	Load	η
C = 28 μF L_g = 10.5 nH V = 2.8 MV τ = 1 μs	L_0 = 4 nH L_1 = 40 nH I_0 = 120 MA	L_z = 7 nH I_z = 60 MA	11.5%

https://doi.org/10.1017/S0263034606060551 Published online by Cambridge University Press

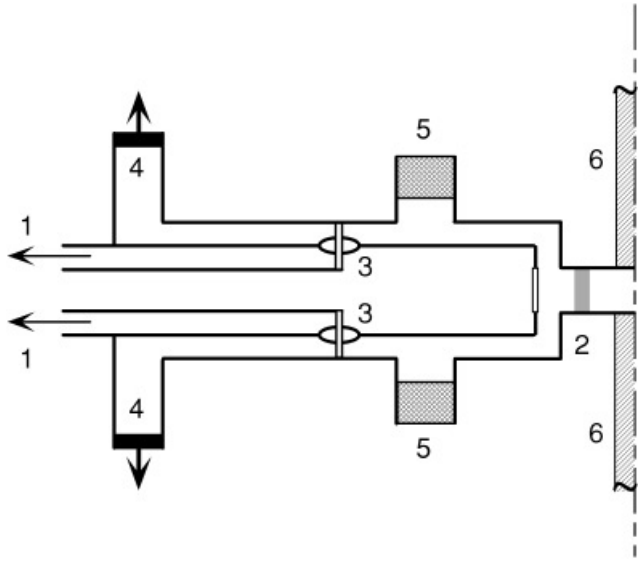

Fig. 5. Parallel connection to a common load. 1—to two capacitor bank, 2—load, 3—convolute, 4—accelerated conductor, 5—closing switches (dielectric flashover), 6—mechanical support.

$$\frac{q}{C} + L_g \frac{dI_g}{dt} + \frac{d}{dt}(L_p I_p) = 0$$

$$\frac{d}{dt}(L_z I_z) + R_s I_z - \frac{d}{dt}(L_p I_p) = 0$$

$$I_g = I_p + I_z. \tag{7}$$

Here C and L_g are the parameters of the capacitive primary storage taken from Table 1. I_g is the generator current; L_p and I_p correspond to the varying inductance and current of the conductor; L_z and I_z are the time-dependent inductance and the current of the load shell. R_s is the resistance of an ideal closing switch connecting L_p and L_z parts ($R_s = \infty$ during the magnetic energy storage time and then $R_s = 0$).

The load was assumed to be a perfectly conducting cylindrical shell accelerated by the magnetic field of the load current I_z and having the mass $m_z = 0.1$ g, the height $h_z = 2$ cm, and the initial radius $r_{ini} = 2.2$ cm.

The conductor 4 in Figure 1 was assumed to be a perfectly conducting foil accelerated by the current I_p and having the mass $M = 0.2$ g. The axial acceleration occurs at the distance $h = 5$ cm in the space between a cathode, $R_c = 50$ cm, and an anode, $R_a = 55$ cm. In order to model the motion of a small current-carrying portion of the conductor mass m shown in Figure 1, the whole conductor mass is divided into two parts at the end of axial acceleration. The mass $M - m$ continues its axial motion. The small mass m is considered as a perfectly conducting cylindrical shell with the height varying in time and equal to $z_M - h$, where $z_M(t)$ is the current position of the main conductor mass. This mass is further radially accelerated by the current I_p.

All the moving parts (load shell and the conductor) participating to the whole scheme operation is described by simple equations of motion

$$M_i \frac{d^2\xi_i}{dt^2} = \frac{I_i^2}{2}\frac{dL_i}{d\xi_i}. \tag{8}$$

Here ξ_i, M_i, and I_i represent accordingly the coordinate, the mass and the current in the described motion, i.e., z, M, and I_p for the main conductor mass; r, m, and I_p for the residual conductor mass compressed radially; r, m_z, and I_z for the load shell. L_i are the varying inductances in corresponding geometries. We also assume a 10-fold radial compression ratio for the masses m and m_z, i.e., their motion is stopped when the masses reach $r = R_c/10$ and $r = r_{ini}/10$ accordingly.

Figures 6 and 7 show the results of numerical solution of the Eqs. (7) and (8) describing the scheme of Figure 1. In the beginning of the capacitor discharge, the current flows through L_g and through the axially accelerated conductor with the mass M. When the conductor passes the length h, the load is connected ($R_s = 0$) and the current starts to flow simultaneously through the shell of residual mass m and through the load shell with the mass m_z. Both masses are imploded radially towards the axis of the system, Figure 1.

The voltage generated during compression of the mass m allows the power flow into the load. There is an uncertainty in quantifying the residual mass value m. This value could be obtained only from more realistic, multi-dimensional numerical modeling. Figures 6 and 7 show the general trend in influence of this parameter on the scheme efficiency. For example, consider $m = 0.01$ M and $m = 0.1$ M. In both cases the load current I_z reaches the maximum value predicted in Section 5 and the generator-to-load energy transfer efficiency is about 10%. However, the higher is the residual mass m, the slower is its compression, the lower is the voltage across the load inductance and the greater is the load current rise-time.

Table 2. *Generator parameters calculated from Figure 4 for parallel connection of two inductive switches shown in Figure 5*

Primary store (1 of 2)	Inductive switch (1 of 2)	Load	η
$C = 22\ \mu$F	$L_0 = 4$ nH	$L_z = 6$ nH	12.3%
$L_g = 14.4$ nH	$L_1 = 40$ nH	$I_z = 60$ MA	
$V = 2.0$ MV	$I_0 = 70$ MA		
$\tau = 1\ \mu$s			

7. CONCLUSION

In conclusion, we described a scheme of pulsed-power conditioning at high currents. In contrast with the resistive opening switches used on inductive energy storage generators, it is suggested to use the voltage of inductive origin obtained through staged acceleration of a solid-state or

https://doi.org/10.1017/S0263034606060551 Published online by Cambridge University Press

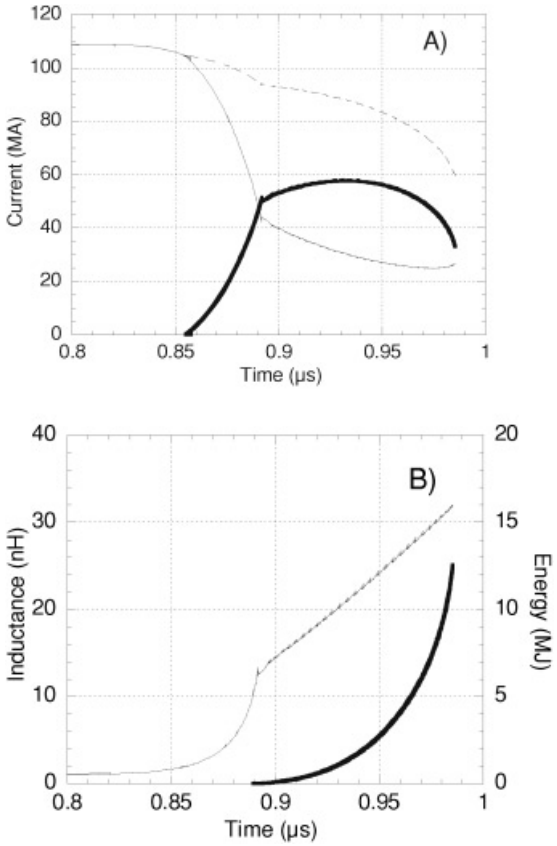

Fig. 6. Circuit modeling result for $m/M = 0.01$. Generator parameters are taken from Table 1. Parameters of the load and of the inductive switch are defined in the text. (a) Currents I_g (dotted), I_p (solid), and I_z (bold); (b) inductance L_p (solid) and the load liner kinetic energy (bold).

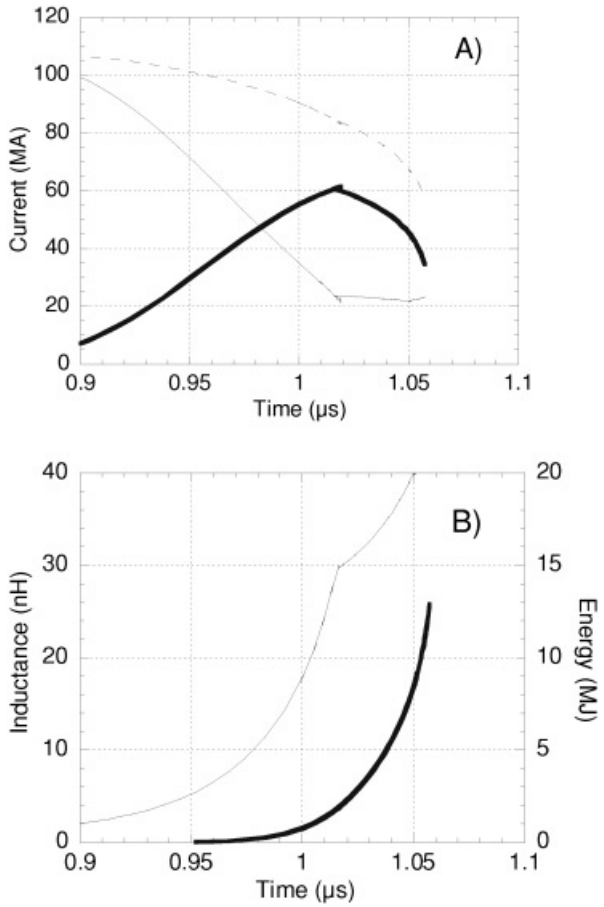

Fig. 7. The same modeling result as for Figure 6 with $m/M = 0.1$.

plasma conductor. Unlike plasma or solid-state resistors, the inductive impedance may increase with the maximum generator current as in the case of fast z-pinch implosions (Matzen, 1997 and the references therein). The conductor must keep low inductance in order to allow efficient energy coupling to a low-impedance primary generator. The conductor must further increase the inductance in order to provide the transfer of magnetic energy to a load. Principle possibility of such a staged acceleration with power multiplication is confirmed experimentally. Further simple analysis based on magnetic flux conservation in the system shows possibility of a 10% generator-to-load energy transfer efficiency for some realistic generator parameters. Possible uncertainties of the scheme operation are identified to be an additional convolute 3, existence of a residual conductor mass m and a closing switch 5, see Figure 1. The latter could represent a controllable low-inductance dielectric flashover switch (e.g., Kokshenev *et al*., 2004). Post-hole convolutes are also shown to operate successfully with z-pinch-type loads at mega-Ampere current levels (Spielman *et al*., 1997). Formation of the residual conductor mass, however, is not studied yet, neither experimentally nor in complicated numerical simulations. We studied the influence of this mass on the scheme efficiency in simple circuit modeling coupled with zero-dimensional equations of motion. The ratio of this mass to the total conductor mass is shown to influence drastically the power multiplication achievable in the scheme.

ACKNOWLEDGMENT

The work was performed under the contract CEG N° 00-25-043-00-470-46-51, Centre d'Etudes de Gramat, France.

REFERENCES

Aleksandrov, V.V., Grabovsky, E.V., Zukakishvili, G.G., Zurin, M.V., Komarov, N.N., Krasovsky, I.V., Mitrofanov, K.N., Nedoseev, S.L., Oleinik, G.M., Porofeev, I. Yu., Samokhin, A.A., Sasorov, P.V., Smirnov, V.P., Fedulov, M.V., Frolov, I.N. & Chernov, A.A. (2003). Current-induced implosion of a multiwire array as a radial plasma rainstorm. *JETP* **97**, 745–753.

Aleksandrov, V.V., Grabovsky, E.V., Zurin, M.V., Krasovsky, I.V., Mitrofanov, K.N., Nedoseev, S.L., Oleinik, G.M., Porofeev, I.Yu., Samokhin, A.A., Sasorov, P.V., Smirnov, V.P., Fedulov, M.V. & Frolov, I.N. (2004). Characteristics of high-power radiating imploding discharge with cold start. *JETP* **99**, 1150–1172.

https://doi.org/10.1017/S0263034606060551 Published online by Cambridge University Press

Chuvatin, A.S., Kim, A.A., Kokshenev, V.A., Kovalchuk, B.M., Kurmaev, N.E., Loginov, S.V. & Fursov, F.I. (1997). A composite POS: First proof-of-principle results from GIT-12. *Proc. 11th IEEE International Pulsed Power Conference*, pp. 261–268. Baltimore: IEEE.

Chuvatin, A.S. (1999). New concept of multi-MA radiation loads in inductive energy storage systems (LL-scheme). *Bull. Am. Phys. Soc.* **44**, 103.

Chuvatin, A.S., Rudakov, L.I., Kokshenev, V.A., Aranchuk, L.E., Huet, D., Gasilov, V.A., Krukovskii, A.Yu., Kurmaev, N.E. & Fursov, F.I. (2002). New IES scheme for power conditioning at ultra-high currents: from concept to MHD modelling and first experiments. *Proc. 5th International Conference on Dense Z-Pinches*, Vol. 651, pp. 47–50. New Mexico: AIP.

Davis, J., Giuliani, Jr., J.L., Rogerson, J. & Thornhill, J.W. (1996). Limitations on the K-shell X-ray conversion efficiency of a krypton Z-Pinch plasma. *Proc. 11th International Conference on High Power Particle Beams*, Vol. II, pp. 709–712. Prague: Tiskarna, Ltd.

IEEETPS (1987). Special issue on Plasma Opening Switches. *IEEE Trans. Plasma Sci.* **PS-15**.

Kokshenev, V.A., Fursov, F.I. & Kurmaev, N.E. (2004). Device for generation of megaampere current pulses with a 10^{-7} s rise time in radiating load of the GIT 12 generator. *Proc. 13th Symp. on High Current Electronics*, pp. 166–169. Tomsk, Russia: Institute of High Current Electronics.

Kovalchuk, B.M., Kokshenev, V.A., Kim, A.A., Kurmaev, N.E., Loginov, S.V. & Fursov, F.I. (1997). GIT16: State of project in 1995–1997. *Proc. 11th IEEE International Pulsed Power Conference*, pp. 715–723. Baltimore: IEEE.

Lebedev, S.V., Beg, F.N., Bland, S.N., Chittenden, J.P., Dangor, A.E., Haines, M.G., Pikuz, S.A. & Shelkovenko, T.A. (1997). Effect of core-corona plasma structure on seeding of instabilities in wire array Z pinches. *Phys. Rev. Lett.* **85**, 98–101.

Matzen, M.K. (1997). Z pinches as intense X-ray sources for high-energy density physics applications. *Phys. Plasmas* **4**, 1519–1527.

Mazarakis, M.G., Deeney, C.E., Douglas, M.R., Stygar, W.A., Sinars, D.B., Cuneo, M.E., Chittenden, J., Chandler, G.A., Nash, T.J., Struve, K.W., & McDaniel, D.H. (2004). Tungsten wire number dependence of the implosion dynamics at the Z-accelerator. *Plasma Devices and Operations* **13**, 157–161.

Megagauss. (1990). *Megagauss fields and pulsed power systems* (Titov, V.M. & Shvetsov, G.A., Eds.). New York: Nova Science Publishers.

Nash, T.J., Deeney, C., Chandler, G.A., Sinars, D.B., Cuneo, M.E., Waisman, E.M., Stygar, W.A., Wenger, D., Speas, S., Leeper, R.J., Seaman, J.F., McGurn, J., Torres, J., Jobe, D., Gilliland, T., Nielsen, D., Hawn, R., Seaman, H., Keller, K., Moore, T., Wagoner, T.C., LePell, P.D., Lucas, J., Schroen, D., Russell, C. & Kernaghan, M. (2004). Comparison of a copper foil to a copper wire-array Z pinch at 18 MA. *Phys. Plasmas* **11**, L65–L68.

Rudakov, L.I. (1999). New loads for pulse power generators. *Proc. 12th IEEE International Pulsed Power Conference*, pp. 1102–1105. Maryland: IEEE.

Rudakov, L.I., Chuvatin, A.S., Velikovich, A. L. & Davis, J. (2003). Confinement and compression of magnetic flux by plasma shells. *Phys. Plasmas* **10**, 4435–4447.

Sinars, D.B., Cuneo, M.E., Yu, E.P., Bliss, D.E., Nash, T.J., Porter, J.L., Deeney, C., Mazarakis, M.G., Sarkisov, G.S. & Wenger, D.F. (2004). Mass-profile and instability-growth measurements for 300-wire *Z*-pinch implosions driven by 14–18 MA. *Phys. Rev. Lett.* **93**, 145002.

Spielman, R.B., Stygar, W.A., Seamen, J.F., Long, F., Ives, H., Garcia, R., Wagoner, T., Struve, K.W., Mostrom, M., Smith, I., Spence, P. & Corcoran, P. (1997). Pulsed power performance of PBFA Z. *Proc. 11th IEEE International Pulsed Power Conference*, pp. 709–714. Baltimore: IEEE.

Turchi, P.J., Alme, M.L., Bird, G., Boyer, C.N., Coffey, S.K., Conte, D., Davis III, J.F. & Seiler, S.W. (1987). Review of plasma flow switch development. *IEEE Trans. Plasma Sci.* **PS-15**, 747–759.

https://doi.org/10.1017/S0263034606060551 Published online by Cambridge University Press